

ARTICLE TEMPLATE

Sum rules for x-ray circular and linear dichroism based on complete magnetic multipole basisY. Yamasaki^{a,b,c}, Y. Ishii^a and N. Sasabe^a^aCenter for Basic Research on Materials, National Institute for Materials Science (NIMS), Tsukuba 305-0047, Japan; ^bInternational Center for Synchrotron Radiation Innovation Smart, Tohoku University, Sendai 980-8577, Japan; ^cCenter for Emergent Matter Science (CEMS), RIKEN, Wako 351-0198, Japan**ARTICLE HISTORY**

Compiled April 24, 2025

ABSTRACT

X-ray magnetic circular dichroism (XMCD) and X-ray magnetic linear dichroism (XMLD) are powerful spectroscopic techniques for probing magnetic properties in solids. In this study, we revisit the XMCD and XMLD sum rules within a complete magnetic multipole basis that incorporates both spinless and spinful multipoles. We demonstrate that these multipoles can be clearly distinguished and individually detected through the sum-rule formalism. Within this framework, the anisotropic magnetic dipole term is naturally derived in XMCD, offering a microscopic origin for ferromagnetic-like behavior in antiferromagnets. Furthermore, we derive the sum rules for out-of-plane and in-plane XMLD regarding electric quadrupole contributions defined based on the complete multipole basis. Our theoretical approach provides a unified, symmetry-consistent framework for analyzing dichroic signals in various magnetic materials. These findings deepen the understanding of XMCD and XMLD and open pathways to exploring complex magnetic structures and spin-orbit coupling effects in emergent magnetic materials.

KEYWORDS

Magnetic materials; X-ray absorption spectroscopy; X-ray magnetic circular dichroism; X-ray magnetic linear dichroism; Altermagnet

1. Introduction**1.1. X-ray absorption spectroscopy**

X-ray absorption spectroscopy (XAS) is a powerful tool for investigating the electronic and magnetic properties of materials [1]. Among its various techniques, X-ray Magnetic Circular Dichroism (XMCD) and X-ray Magnetic Linear Dichroism (XMLD) have been extensively applied in synchrotron-based experiments to investigate element-specific information on magnetism [2–5]. XMCD is a phenomenon where the absorption of circularly polarized X-rays differs depending on the relative orientation of the photon helicity and the magnetization. This effect arises from the spin-orbit interaction in the core-level states, leading to different transition probabilities for left- and right-circularly polarized light. XMCD is widely used to determine element-specific spin and

orbital magnetic moments via sum rules [6–9]. It has been extensively applied to transition metal and rare-earth compounds to study magnetic ordering, local electronic structure, and hybridization effects. XMCD has played a crucial role in understanding magnetic thin films, multilayers, and nanostructures, especially in spintronics and permanent magnets [5, 10–13]. Due to its sensitivity to both spin and orbital contributions to magnetism, XMCD enables separating these components [14], which is essential for studying phenomena such as spin-orbit coupling and anisotropy in magnetic materials.

In contrast to XMCD, XMLD refers to the difference in X-ray absorption between two orthogonal linear polarizations in a magnetically ordered system [15, 16]. XMLD is primarily sensitive to the anisotropy of the local electronic structure and provides information about orbital occupation and magnetic ordering. Unlike XMCD, which directly probes net magnetization, XMLD is particularly useful for investigating antiferromagnetic and non-collinear magnetic structures. XMLD arises from the anisotropic valence state due to the spin-orbit and exchange interactions, leading to an anisotropic absorption cross-section. This makes XMLD a valuable tool for studying magnetocrystalline anisotropy, spin reorientation transitions, and antiferromagnetic domain structures in materials such as transition metal oxides and rare-earth compounds.

1.2. *Altermagnet*

Recent advances in spintronics have led to the discovery and investigation of a new class of antiferromagnetic materials known as altermagnets [17–24]. These materials exhibit a unique band structure that combines characteristics of both ferromagnets and antiferromagnets. While the net magnetization vanishes in real space, significant spin splitting emerges in momentum space due to symmetry constraints. Traditionally, X-ray magnetic circular dichroism (XMCD) has served as a powerful tool for probing the magnetic properties of ferromagnetic and ferrimagnetic materials. However, recent theoretical and experimental studies have demonstrated that XMCD can also yield valuable insights into antiferromagnets, even in the absence of net magnetization [25–29]. In such systems, XMCD signals do not originate from conventional magnetization but instead arise from magnetic multipoles, particularly the so-called T_z term, which represents the anisotropic magnetic dipole moment.

The emergence of XMCD via the T_z term in antiferromagnets was theoretically predicted and experimentally confirmed in Mn_3Sn . The origin of this XMCD signal lies in a cluster-scale spin asymmetry in the Mn sublattice, described by the cluster magnetic octupole—a form of augmented magnetic multipole. A similar mechanism operates in RuO_2 , a collinear antiferromagnet identified as an altermagnet. Although it exhibits zero net magnetization, the crystal symmetry permits a residual anisotropic magnetic dipole moment to remain uncanceled, thus enabling XMCD detection. This behavior has been supported by both theoretical analysis and computational studies. Furthermore, XMCD signals were recently observed in collinear antiferromagnetic MnTe [30, 31], and the XMCD can be attributed to the T_z term. Overall, the emergence of XMCD in antiferromagnets is best understood not in terms of net magnetization but within the framework of augmented magnetic multipoles. Therefore, it is essential to interpret XAS, XMCD, and XMLD within the context of the magnetic multipole basis.

(s, k)	$(1, -1)$	$(1, 0)$	$(1, 1)$
$Q_{00}^{(s,k)}$	-	-	$-C_{1,m-n;1n}^{00} M_{1,m-n}^{(\text{orb})} \sigma_{1n}$
$M_{1m}^{(s,k)}$	$C_{0,m-n;1n}^{1m} Q_{0,m-n}^{(\text{orb})} \sigma_{1n}$	$iC_{1,m-n;1n}^{1m} G_{1,m-n}^{(\text{orb})} \sigma_{1n}$	$-C_{2,m-n;1n}^{1m} Q_{2,m-n}^{(\text{orb})} \sigma_{1n}$
$Q_{2m}^{(s,k)}$	$C_{1,m-n;1n}^{2m} M_{1,m-n}^{(\text{orb})} \sigma_{1n}$	$iC_{2,m-n;1n}^{2m} T_{2,m-n}^{(\text{orb})} \sigma_{1n}$	$-C_{3,m-n;1n}^{2m} M_{3,m-n}^{(\text{orb})} \sigma_{1n}$

Table 1. Classification of spinful multipoles ($s = 1$) with the inversion symmetry, *i.e.* electric monopole, magnetic dipole, and electric quadrupole moment, for possible k parameters.

1.3. Complete multipole basis

Multipole expansions systematically describe various physical properties, such as charge and magnetic distributions, in condensed matter systems. The conventional classification distinguishes between electric multipoles \mathbf{Q} (arising from charge distributions) and magnetic multipoles \mathbf{M} (associated with current and spin distributions). However, recent developments by Hayami and Kusunose *et al.*, have established a complete magnetic multipole basis that extends this classification to include electric toroidal multipoles \mathbf{G} and magnetic toroidal multipoles \mathbf{T} [32, 33]. The multipole representation of four-type multipoles enables a comprehensive understanding of various electronic properties and physical phenomena observed in materials.

The general form of a multipole operator in spinless Hilberlt space is expressed as $\hat{X}_{lm}^{(\text{orb})}$ where l and m denote the quantum numbers of the orbital angular momentum, and X represents the type of multipole ($X = \mathbf{Q}, \mathbf{M}, \mathbf{T}, \mathbf{G}$). The multipole operator in the spinful space is obtained by angular momentum coupling between the spinless multipole and the spin angular momentum [32, 33], which is given by

$$\hat{X}_{lm}^{(s,k)} \equiv i^{s+k} \sum_{n=-s}^s C_{l+k,m-n;sn}^{lm} \hat{X}_{l+k,m-n}^{(\text{orb})} \hat{\sigma}_{sn} \quad (1)$$

where $C_{l_1,m_1;l_2,m_2}^{lm}$ is the Clebsh-Gordan coefficient, $s = 0, 1$ and $-s \leq k \leq s$ (k is integer). The spin operator is expressed using the Pauli matrices σ_{sn} in the spin space, defined as $\sigma_{00} = \sigma_0$ (the identity matrix), $\sigma_{10} = \sigma_z$, and $\sigma_{1,\pm 1} = \mp(\sigma_x \pm i\sigma_y)/\sqrt{2}$. Magnetic multipoles are classified based on their transformation properties under spatial inversion (\mathcal{I}) and time-reversal (\mathcal{T}) symmetry. In this paper, we focus only on multipoles that possess spatial inversion symmetry (\mathcal{I}), namely, electric monopoles Q_{00} , magnetic dipoles M_{1m} , and electric quadrupoles Q_{2m} .

Spinless multipoles ($s = 0$) are expressed as $\hat{X}_{lm}^{(0,0)} \equiv \hat{X}_{lm}^{(\text{orb})} \sigma_0$. Since σ_0 is the identity matrix, the type of magnetic multipole basis coincides with that of the orbital multipole basis, namely, $\hat{Q}_{lm}^{(0,0)} = \hat{Q}_{lm}^{(\text{orb})}$ and $\hat{M}_{lm}^{(0,0)} = \hat{M}_{lm}^{(\text{orb})}$. On the other hand, in the spinful space ($s = 1$), since the time-reversal symmetry of spin is odd, the time-reversal symmetry of $\hat{X}_{lm}^{(1,k)}$ should be opposite to that of $\hat{X}_{lm}^{(\text{orb})}$. In addition, since the spin is the axial vector, a spinful multipole is composed of orbital multipoles with different spatial parity. For example, the electric multipole ($\hat{X} = \hat{Q}$) contains three

spinful multipoles ($s = 1, k = -1, 0, 1$),

$$\hat{Q}_{lm}^{(1,0)} = i \sum_n C_{l,m-n;1n}^{lm} \hat{T}_{l,m-n}^{(orb)} \hat{\sigma}_{1n}, \quad (2)$$

$$\hat{Q}_{lm}^{(1,\pm 1)} = i^{1\pm 1} \sum_n C_{l\pm 1,m-n;1n}^{lm} \hat{M}_{l\pm 1,m-n}^{(orb)} \hat{\sigma}_{1n}, \quad (3)$$

suggesting that spinful charge multipoles are generated from the combination of magnetic toroidal moments with the same l (\hat{T}_l) and magnetic multipoles with l differing by one ($\hat{M}_{l\pm 1}$). As well as, the magnetic multipole ($\hat{X} = \hat{M}$) has

$$\hat{M}_{lm}^{(1,0)} = i \sum_n C_{l,m-n;1n}^{lm} \hat{G}_{l,m-n}^{(orb)} \sigma_{1n}, \quad (4)$$

$$\hat{M}_{lm}^{(1,\pm 1)} = i^{1\pm 1} \sum_n C_{l\pm 1,m-n;1n}^{lm} \hat{Q}_{l\pm 1,m-n}^{(orb)} \sigma_{1n}, \quad (5)$$

indicating that spinful charge multipoles are generated from the combination of electronic toroidal moments with the same l (\hat{G}_l) and electric charge multipoles with l differing by one ($\hat{Q}_{l\pm 1}$). The relationship between these complete magnetic multipole bases and the spinless and spinful bases is summarized in Table 1.

The matrix element of $\hat{X}_{lm}^{(s,k)}$ on $|l_v, m_v; \frac{1}{2}m_s\rangle$ basis is given by

$$\langle l_v m'_v; \frac{1}{2}m'_s | \hat{X}_{lm}^{(s,k)} | l_v m_v; \frac{1}{2}m_s \rangle = i^{s+k} C_{\kappa\mu;sn}^{lm} C_{l_v m'_v; \kappa\mu}^{l_v m'_v} C_{\frac{1}{2}m_s;sn}^{\frac{1}{2}m'_s} \frac{\langle l_v || \hat{X}_\kappa^{(orb)} || l_v \rangle}{\sqrt{2l_v + 1}} \quad (6)$$

with $\kappa \equiv l + k$ and $\mu \equiv m - n$. $\langle l_v || \hat{X}_\kappa^{(orb)} || l_v \rangle$ is the reduced matrix element, whose explicit expression for $X = Q$ and M are given in Eqs. (8) and (9) in Ref. [32]. Using the spherical tensor for multipole for $l = 0, 1, 2, \dots$ and its z -component $m = -l, -l + 1, \dots, l$,

$$O_{lm} \equiv \sqrt{\frac{4\pi}{2l + 1}} r^l Y_{lm}(\hat{r}) \quad (7)$$

with $\hat{r} = \mathbf{r}/r$ and the spherical harmonics Y_{lm} , the electronic and magnetic multipoles are given by $Q_{lm}^{(orb)} = O_{lm}$ and

$$M_{l,m}^{(orb)} = \frac{1}{2} [(\nabla O_{lm}) \cdot \hat{m}_l + \hat{m}_l \cdot (\nabla O_{lm})] \quad (8)$$

with $\hat{m}_l = 2\hat{l}/(l + 1)$, respectively. For example, ∇O_{lm} corresponding to the magnetic dipole ($l = 1$) and octupole ($l = 3$) can be explicitly given in Table 2.

2. Theoretical Framework of X-ray absorption

In recent decades, the development of sum rules for X-ray absorption spectroscopy has significantly advanced our understanding of the electronic and magnetic properties. Sum rules link the integrated intensity of XAS and dichroism spectra to ground-state

(l, m)	∇O_{lm}
$(1, \pm 1)$	$\mp \frac{1}{2}(e_x \pm ie_y)$
$(1, 0)$	e_z
$(3, \pm 3)$	$\mp \frac{3\sqrt{5}}{4}(x \pm iy)^2(e_x \pm ie_y)$
$(3, \pm 2)$	$\frac{1}{2}\sqrt{\frac{15}{2}}(x \pm iy)[2z(e_x \pm ie_y) + (x \pm iy)e_z]$
$(3, \pm 1)$	$\mp \frac{\sqrt{3}}{4}[(5z^2 - r^2)(e_x \pm ie_y) + 2(x \pm iy)(5ze_z - r)]$
$(3, 0)$	$-3z(xe_x + ye_y) + \frac{3}{2}(3z^2 - r^2)e_z$

Table 2. Explicit expression of ∇O_{lm} relating magnetic dipole ($l = 1$) and octupole ($l = 3$) with the position operator $\mathbf{r} = (x, y, z)$ and the unit vector $\mathbf{e} = (e_x, e_y, e_z)$.

quantities such as spin, orbital magnetic moments, and charge distribution. These relationships have provided profound insights into magnetic anisotropy, spin-orbit coupling, and electronic correlations. This work presents sum rules for X-ray absorption based on the complete magnetic multipole bases.

The theoretical framework for X-ray absorption for electric dipole transition is rooted in the Fermi Golden Rule, which relates the absorption coefficient to the transition probability $\mu_\varepsilon(\hbar\omega)$ defined by

$$\mu_\varepsilon(\hbar\omega) \equiv \sum_{f, M} |\langle \psi_f | \mathbf{E} \cdot \mathbf{r} | \psi_g \rangle|^2 \delta(E_f - E_g - \hbar\omega), \quad (9)$$

with polarization vector $\mathbf{E} = E_0 \varepsilon$ of the incident x-ray polarization and position operator \mathbf{r} . They can be expanded as the vector product in terms of spherical tensor operators,

$$\mathbf{E} \cdot \mathbf{r} = E_0 \sum_{M=-1}^1 (-1)^M \varepsilon_{-M} r_M \quad (10)$$

where r_M is the spherical tensors of rank 1, and $\varepsilon_{\pm 1} = \mp(\varepsilon_x \pm i\varepsilon_y)/\sqrt{2}$ and $\varepsilon_0 = \varepsilon_z$, corresponding to the circular and linear polarization, respectively. E_g (E_f) indicates the energy of initial (final) states, and $\hbar\omega$ is the photon energy. $|\psi_g\rangle = |\psi(l_v^n)\rangle$ denotes any state of the ground configuration of the outer shell, *i.e.* a valence electronic state of n electrons with the azimuthal angular momentum l_v . The final state configuration is represented by $|\psi_f\rangle = |\underline{c}_{jm} \psi'(l_v^{n+1})\rangle$ where \underline{c}_{jm} stands for a hole in a core level. This formulation captures the core-level transitions induced by the electric multipole interaction, which dominates in XAS experiments.

The integral of XAS concerning the electric dipole transition from a core state with $j_\pm = l_c \pm \frac{1}{2}$ is expressed as

$$I_\varepsilon^{j\pm} = \int_{j_\pm} \mu_\varepsilon(\hbar\omega) d\omega = \sum_{MM'} E_0^2 (-1)^{M+M'} \varepsilon_{-M}^* \varepsilon_{-M} P_{M'M}^{j\pm} \quad (11)$$

with

$$P_{M'M}^{j\pm} \equiv \sum_{f \in j_\pm} \langle \psi_g | r_{M'} | \psi_f \rangle \langle \psi_f | r_M | \psi_g \rangle. \quad (12)$$

Using the Wigner-Eckart theorem, the matrix element of photoelectron transition from the core state jm_j to the valence state $l_v m_v$ by the electric dipole moment r_M is given by

$$\langle \psi_f | r_M | \psi_g \rangle = \sum_{\{m\}} C_{l_c m_c; 1M}^{l_v m_v} C_{l_c m_c; \frac{1}{2} m_s}^{j m_j} \frac{\langle \psi_f | a_{m_v m_s}^\dagger b_{j m_j} | \psi_g \rangle}{\sqrt{2l_v + 1}} \langle l_v | |O_1| |l_c \rangle_R \quad (13)$$

where $C_{l_1 m_1; l_2 m_2}^{l_3 m_3}$ is the Clebsh-Gordan coefficient and the index of $\{m\}$ indicates the summation for all m . $\langle l_v | |O_1| |l_c \rangle_R$ denotes the reduced matrix element independent of any m .

By substituting Eq. (13) into Eq. (12), $P_{M'M}^{j\pm}$ can be rewritten as

$$P_{M'M}^{j\pm} = \sum_{\psi_f} \sum_{\{m\}} [l_v]^{-1} C_{l_c m_c; 1M}^{l_v m_v} C_{l_c m_c; \frac{1}{2} m_s}^{j m_j} C_{l_c m'_c; 1M'}^{l_v m'_v} C_{l_c m'_c; \frac{1}{2} m'_s}^{j m'_j} \times \langle \psi_g | b_{j m_j}^\dagger a_{m_v m_s} | \psi_f \rangle \langle \psi_f | a_{m'_v m'_s}^\dagger b_{j m'_j} | \psi_g \rangle R_{l_c} \quad (14)$$

with $[l_v] \equiv 2l_v + 1$ and $R_{l_c} = |\langle l_v | |O_1| |l_c \rangle_R|^2$. By taking the sum over m_j while noting that $m'_j = m_j$ for the absorption process, we arrive at the following equation [34]:

$$P_{M'M}^{j\pm} = \sum_{\{m\}} \sum_{s=0}^1 \sum_{n=-s}^s \frac{\alpha_\pm^{(s)}(l_c)}{[l_c l_v]} C_{l_c m_c; 1M}^{l_v m_v} C_{l_c m'_c; 1M'}^{l_v m'_v} C_{l_c m'_c; s, -n}^{l_c m_c} C_{\frac{1}{2} m'_s; sn}^{\frac{1}{2} m_s} \times \langle \psi_g | a_{m_v m_s} a_{m'_v m'_s}^\dagger | \psi_g \rangle R_{l_c} \quad (15)$$

with $[ab \cdots] \equiv (2a+1)(2b+1) \cdots$. Here, $\alpha_\pm^{(s)}(l_c)$ is a coefficient depending on the core state $j_\pm = l_c \pm 1/2$ and expressed as

$$\alpha_\pm^{(s)}(l_c) = \begin{cases} j_\pm + \frac{1}{2} & (s=0) \\ \pm \sqrt{3l_c(l_c+1)} & (s=1). \end{cases} \quad (16)$$

This parameter implies that the absorption intensity can be divided into processes in which the spin does not flip ($s=0$) and those where the spin flips ($s=1$). By summing the absorption intensities from both j_\pm , the spin-flip processes cancel out, leaving only the information from the spin nonflip process. By calculating the absorption intensity for j_\pm separately and taking the appropriate difference, the information on the spin-flop process can be obtained. In other words, observing the absorption process of the spin-flop transition requires absorption in the inner core levels split by the spin-orbit interaction.

3. Polarization Sum rules of X-ray absorption

To relate X-ray absorption to the physical symmetry of the holes in the valence state, here, we introduce a multipole with the quantum numbers l and m defined as

$$S_{lm}^{j\pm} \equiv \sum_{MM'} C_{1M'; lm}^{1M} P_{M'M}^{j\pm}, \quad (17)$$

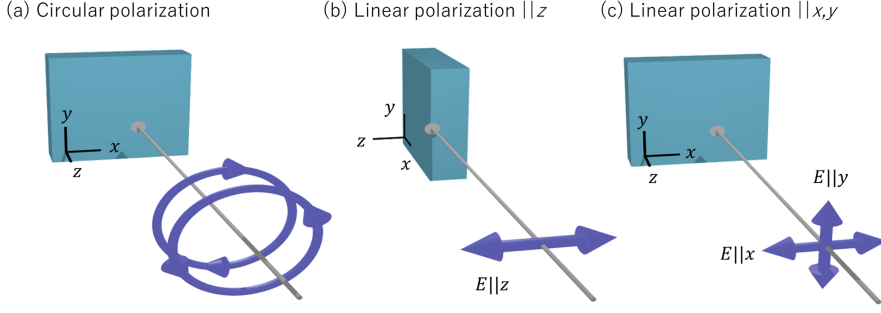


Figure 1. Experimental setup of x-ray absorption with the incident polarization of (a) circular, (b) linear ($E||z$), and (c) linear ($E||x$ and $E||y$).

giving some descriptions of the sum of XAS with different X-ray polarizations. The sum of XAS for isotropic polarization is linked to the electric monopole, which is confirmed by $S_{00}^{j\pm} = I_z^{j\pm} + I_+^{j\pm} + I_-^{j\pm}$ due to $C_{1M';00}^{1M} = \delta_{MM'}$. The dipole moment quantum number gives $S_{10}^{j\pm} = \frac{1}{\sqrt{2}}(I_-^{j\pm} - I_+^{j\pm})$ due to $C_{1M';10}^{1M} = \frac{1}{\sqrt{2}}M\delta_{MM'}$, which corresponds to XMCD when the incident X-ray is aligned along the z axis. In addition, we consider (i) perpendicular and (ii) in-plane X-ray magnetic linear dichroism (XMLD). The perpendicular XMLD is expressed by a quadrupole moment $S_{20}^{j\pm} = \frac{1}{\sqrt{10}}(I_+^{j\pm} + I_-^{j\pm} - 2I_z^{j\pm})$, representing the difference in XAS with linear polarization between the perpendicular and in-plane directions. In contrast, the in-plane XMLD, i.e., the difference in XAS with linear polarization between the in-plane x - and y -directions, can not be described by a single S_{lm} . However, using a relation of $S_{2,\pm 2}^{j\pm} = \frac{3}{\sqrt{15}}P_{\pm 1,\mp 1}^{j\pm}$, it is confirmed that its difference is linked to the in-plane XMLD as $S_{2,2}^{j\pm} + S_{2,-2}^{j\pm} = \frac{3}{\sqrt{15}}(I_y^{j\pm} - I_x^{j\pm})$ as discussed below.

Substituting Eq. (12) into Eq. (17) results in a product of four Clebsch-Gordan coefficients involving summation over m_c, m'_c, M , and M' . By applying the transformation formula for the Wigner-9j symbol [35], Equation (17) can be rewritten as

$$S_{lm}^{j\pm} = \sum_{s,\kappa} \sum_{n,\mu} \sum_{\{m\}} \alpha_{\pm}^{(s)} \beta_l^{(s,\kappa)} \langle \psi_g | C_{\kappa\mu;sn}^{lm} C_{l_v m'_v; \kappa\mu}^{l_v m_v} C_{\frac{1}{2}m'_s;sn}^{\frac{1}{2}m_s} a_{m_v m_s} a_{m'_v m'_s}^\dagger | \psi_g \rangle \quad (18)$$

where $s = 0, 1$ and $|s - l| \leq \kappa \leq \min(2l_v, s + l)$ (κ is integer). The coefficient $\beta_l^{(s,\kappa)}$ is independent of any m and expressed using the Wigner-9j symbol as

$$\beta_l^{(s,\kappa)}(l_c, l_v, L) \equiv \frac{[\kappa][L]^{\frac{1}{2}}}{[l_c l_v l]^{\frac{1}{2}}} \begin{Bmatrix} l_v & l_c & L \\ l_v & l_c & L \\ \kappa & s & l \end{Bmatrix} R_{l_c} \quad (19)$$

where $[ab\cdots]^{\frac{1}{2}} \equiv \{(2a+1)(2b+1)\cdots\}^{\frac{1}{2}}$ and $\{\cdot\cdots\}$ indicate the Wigner-9j symbols. Here, we consider a complete multipole operator for holes in the valence of the ground state $|\psi_g\rangle$ expressed by $\hat{X}_{lm}^{(s,k)}$ based on the analogy of Eq. (1). Consequently, the sum of XAS at $j_{c\pm} = l_c \pm \frac{1}{2}$ core state can be rewritten by using the expectation value of

Technique	l	m	s	k	multipole basis	sum rule
XAS	0	0	0	0	$Q_{00}^{(orb)} \sigma_0$	n_h
			1	1	$M_{1,-n}^{(orb)} \sigma_{1n}$	$\hat{\mathbf{l}} \cdot \hat{\mathbf{s}}$
XMCD	1	m	0	0	$M_{1,m}^{(orb)} \sigma_0$	\underline{l}_z
			1	-1	$Q_{0,0}^{(orb)} \sigma_{1n}$	\underline{s}_z
			1	1	$Q_{2,m-n}^{(orb)} \sigma_{1n}$	$[\underline{\mathbf{Q}} \otimes \underline{\mathbf{s}}]_z$
XMLD	2	m	0	0	$Q_{2,m}^{(orb)} \sigma_0$	$\underline{Q}_{zz}, \underline{Q}_{x^2-y^2}$
			1	-1	$M_{1,m-n}^{(orb)} \sigma_{1n}$	$[\underline{\mathbf{l}} \otimes \underline{\mathbf{s}}]_z$
			1	1	$M_{3,m-n}^{(orb)} \sigma_{1n}$	$[\underline{\mathbf{M}}_3^{(orb)} \otimes \underline{\mathbf{s}}]_z$

Table 3. Classification of sum rules for X-ray absorption spectrum (XAS), X-ray magnetic circular dichroism (XMCD), and X-ray magnetic linear dichroism (XMLD) based on the complete multipole basis.

complete magnetic multipoles for holes and Eq. (6) as

$$S_{lm}^{j\pm} = \alpha_{\pm}^{(0)} \beta_l^{(0,l)} \langle \underline{X}_{lm}^{(0,0)} \rangle + \alpha_{\pm}^{(1)} \beta_l^{(1,l-1)} \langle \underline{X}_{lm}^{(1,-1)} \rangle - \alpha_{\pm}^{(1)} \beta_l^{(1,l+1)} \langle \underline{X}_{lm}^{(1,1)} \rangle, \quad (20)$$

with $\langle \underline{X}_{lm}^{(s,k)} \rangle \equiv \sum_{n,\mu} \sum_{\{m\}} i^{s+k} \langle \psi_g | C_{\kappa\mu;sn}^{lm} C_{l_v m'_v; \kappa\mu}^{l_v m_v} C_{\frac{1}{2} m'_s;sn}^{\frac{1}{2} m_s} a_{m_v m_s} a_{m'_v m'_s}^\dagger | \psi_g \rangle$. Since $\langle \underline{X}_{lm}^{(s,k)} \rangle$ contains only the expectation value for angular information of the complete multipole basis, it can be represented by equivalent operators [36]. Noted that the Wigner-9j symbol in Eq. (19) becomes zero when $s = 1$ and $k = l$, and therefore $\beta_l^{(1,l)} = 0$. This means that the sum rule of dipole transition can capture the information for electric and magnetic multipoles, \mathbf{Q} and \mathbf{M} on a complete magnetic multipole basis, and cannot directly apply to electric and magnetic toroidal moments, \mathbf{G} and \mathbf{T} .

Using the relations $\alpha_{+}^{(1)} + \alpha_{-}^{(1)} = 0$, the sum over $S_{lm}^{j\pm}$ on the two core states $j_{\pm} = l_c \pm \frac{1}{2}$ is expressed as,

$$S_{lm}^{j+} + S_{lm}^{j-} = [l_c] \beta_l^{(0,l)} \langle \underline{X}_{lm}^{(0,0)} \rangle, \quad (21)$$

suggesting that it gives expectation values for the spinless multipoles. Hereafter, it will be referred to as the spinless sum rule. Similarly, by using a relation $\alpha_{+}^{(0)} - \frac{l_c+1}{l_c} \alpha_{-}^{(0)} = 0$, another sum rule can be derived,

$$S_{lm}^{j+} - \frac{l_c+1}{l_c} S_{lm}^{j-} = [l_c] \sqrt{\frac{3(l_c+1)}{l_c}} \left\{ \beta_l^{(1,l-1)} \langle \underline{X}_{lm}^{(1,-1)} \rangle - \beta_l^{(1,l+1)} \langle \underline{X}_{lm}^{(1,1)} \rangle \right\}, \quad (22)$$

which allows for the detection of only spinful multipoles. Hereafter, it will be referred to as the spinful sum rule. In other words, depending on the method of calculating the absorption sum with the core as the reference, it is possible to extract either spinless or spinful magnetic multipoles selectively.

4. Explicit expression of magnetic multipoles in sum rules

In the present paper, we will examine the relationship between the XAS, XMCD, and XMLD sum rules, and magnetic multipoles concretely using the case of the dipole transition $l_c = 1$ ($2p$ orbitals) $\rightarrow l_v = 2$ ($3d$ orbitals) as an example. The relation between the polarization sum rules and the complete magnetic multipole basis and physical quantity is classified in Table 3.

4.1. Monopole sum rule

The sum rule on the isotropic XAS ($I_{\text{XAS}}^{j\pm} = I_z^{j\pm} + I_+^{j\pm} + I_-^{j\pm}$) gives the complete multipole basis of charge monopole $l = 0, m = 0$. Since the spinless monopole is given by $\underline{Q}_{00}^{(0,0)} = Q_{00}^{(\text{orb})} = O_{00}$, the spinless sum rule ($s = 0$) is expressed as

$$I_{\text{XAS}}^{j+} + I_{\text{XAS}}^{j-} = \langle n_h \rangle C, \quad (23)$$

where n_h indicates the number of holes in the l_v state and C is the normalized constant factor including the radial matrix element of the dipole transition and multipoles. On the other hand, the spinful monopole is given by

$$Q_{00}^{(1,1)} = - \sum_n C_{1,-n;1,n}^{00} M_{1,-n}^{(\text{orb})} \sigma_{1n} = \frac{1}{\sqrt{3}} (\hat{\mathbf{l}} \cdot \hat{\mathbf{s}}), \quad (24)$$

which involves the spin-orbit coupling ($\lambda \hat{\mathbf{l}} \cdot \hat{\mathbf{s}}$) in the l_v state. Consequently, the intensity of the spinful monopole sum rule is proportional to $Q_{00}^{(1,1)}$, and is expressed as

$$I_{\text{XAS}}^{j+} - 2I_{\text{XAS}}^{j-} = \langle \hat{\mathbf{l}} \cdot \hat{\mathbf{s}} \rangle C, \quad (25)$$

where C is the same normalized factor as in Eq. (23). This means that when the spin-orbit interaction in l_v is zero, the intensity ratio of I_{XAS}^{j+} to I_{XAS}^{j-} is 2:1, and conversely, as the interaction becomes stronger, the absorption intensity of I_{XAS}^{j-} decreases.

4.2. Dipole sum rule

The sum rule for $l = 1$ represents that for the XMCD spectrum ($I_{\text{XMCD}}^{j\pm} = I_+^{j\pm} - I_-^{j\pm}$) and involves the first-order multipoles associated with the magnetic dipole moment. Here, we consider $m = 0$, that is, $S_{10}^{j\pm} = -\frac{1}{\sqrt{2}}(I_+^{j\pm} - I_-^{j\pm})$, which gives the component of each dipole moment projected onto the z direction. Since the spinless dipole moment is given by $\underline{M}_{10}^{(0,0)} = M_{10}^{(\text{orb})} = l_z$, the spinless sum rule ($s = 0$) is expressed as

$$I_{\text{XMCD}}^{j+} + I_{\text{XMCD}}^{j-} = -\frac{1}{2} \langle l_z \rangle C, \quad (26)$$

indicating that the sum rule of the XMCD selectively extracts information on orbital angular momentum in magnetization [6].

On the other hand, spinful dipole moments have two components: one is the pure spin represented by $\underline{M}_{10}^{(1,-1)} = C_{00;10}^{10} \underline{Q}_{00}^{(\text{orb})} \underline{\sigma}_z = \underline{\sigma}_z$, and the other is a term arising

from the coupling between the electric quadrupole and the spin,

$$[M_{10}^{(1,1)}]_z = - \sum_n C_{2,-n;1n}^{10} Q_{2,-n}^{(\text{orb})} \sigma_{1n} = \frac{1}{\sqrt{10}} \sum_i (3zr_i - \mathbf{r}^2 \delta_{zr_i}) \sigma_z \quad (27)$$

with \mathbf{r} being operators for the unit vector of position [33]. The latter is proportional to the anisotropic magnetic dipole t_z term [37], which provides information on the anisotropy of the electron spin-density distribution. Consequently, the spinful sum rule ($s = 1$) is expressed as

$$I_{\text{XMCD}}^{j+} - 2I_{\text{XMCD}}^{j-} = - \left(\frac{2}{3} \langle \underline{s}_z \rangle + \frac{7}{3} \langle t_z \rangle \right) C, \quad (28)$$

with $t_z = \frac{1}{4} (3[l_z(\mathbf{l} \cdot \mathbf{s})]_+ - 2l^2 s_z)$ in the the equivalent l orperator form [38]. The t_z term has recently been identified as a key origin of XMCD signals in antiferromagnets lacking net magnetization, as exemplified by Mn₃Sn [25, 26] and collinear antiferromagnetic systems [39], and also plays an important role in the anomalous Hall effect in antiferromagnet [40].

4.3. Quadrupole sum rule for out-of-plane XMLD ($z\text{XMLD}$)

The sum rule for $l = 2$ represents that for the XMLD spectrum and involves the second-order multipoles associated with the electronic quadrupole moment. First, we consider $m = 0$, that is, $S_{20}^{j\pm} = \frac{1}{\sqrt{10}} (I_+^{j\pm} + I_-^{j\pm} - 2I_z^{j\pm})$, which shows the difference in x-ray absorption intensity when the polarization is applied within the xy plane and along the out-of-plane direction [see Fig. 1(a) and (b)]. The spinless multipole of the quadrupole moment is given by $\underline{Q}_{20}^{(0,0)} = \underline{Q}_{20}^{(\text{orb})}$, which represents the electronic quadrupole moment $O_{20} = \frac{1}{2} (3z^2 - r^2)$, corresponding to $d_{3z^2-r^2}$ orbital. Therefore, the spinless sum rule ($s = 0$) is expressed as,

$$I_{z\text{XMLD}}^{j+} + I_{z\text{XMLD}}^{j-} = \langle \underline{Q}_{zz} \rangle C, \quad (29)$$

with the equivalent operator $\underline{Q}_{zz} = \frac{1}{2} (l_z^2 - \frac{1}{3} l^2)$ [36]. This result reflects the anisotropy of charge distribution between the out-of-plane and the in-plane direction.

The spinful electronic quadrupole moments are composed of magnetic dipole and octupole terms. The magnetic dipole one is given by

$$Q_{20}^{(1,-1)} = \sum_n C_{1,-n;1n}^{2,0} M_{1,-n}^{(\text{orb})} \sigma_{1n} = \frac{1}{\sqrt{6}} (3l_z s_z - \mathbf{l} \cdot \mathbf{s}), \quad (30)$$

indicating the anisotropy of the spin-orbit coupling ($\lambda \mathbf{l} \cdot \mathbf{s}$), which enables the probing of the magnetocrystalline anisotropy [41]. The equivalent operator is given by $P_{zz} = \frac{1}{2} (3l_z s_z - \mathbf{l} \cdot \mathbf{s})$ [36, 38]. The octupole term in the spinful quadrupole moment is expressed as

$$Q_{20}^{(1,1)} = - \sum_n C_{3,-n;1n}^{2,0} M_{3,-n}^{(\text{orb})} \sigma_{1n} \quad (31)$$

where the magnetic octupole operators are shown in the Table 2. For example, when

the spin is oriented along the z -axis, the explicit expression by extracting only the term proportional to s_z is given by

$$M_{30}^{(\text{orb})} \sigma_z = -\frac{3}{2} [zx l_x + zy l_y]_+ s_z + \frac{3}{2} (3z^2 - r^2) l_z s_z \quad (32)$$

which reflects a quantity combining the electric quadrupole and spin-orbit coupling. Consequently, the spinful sum rule is expressed as,

$$I_{z\text{XMLD}}^{j+} - 2I_{z\text{XMLD}}^{j-} = \left(\frac{2}{5} \langle \underline{P}_{zz} \rangle + \frac{3}{5} \langle \underline{R}_{zz} \rangle \right) C, \quad (33)$$

where $R_{zz} = \frac{1}{3} [5l_z(\mathbf{l} \cdot \mathbf{s})l_z - (l^2 - 2)\mathbf{l} \cdot \mathbf{s} - (2l^2 + 1)l_z s_z]$ is the equivalent operator of $Q_{20}^{(1,1)}$ [36, 38]. In the case of the electric quadrupole sum rule, it is difficult to separately measure the spinful magnetic dipole and magnetic octupole. As a result, it is also useful to express as $I_{z\text{XMLD}}^{j+} - 2I_{z\text{XMLD}}^{j-} = \langle \underline{U}_{zz} \rangle C$ using the total operator $U_{zz} = l_z(\mathbf{l} \cdot \mathbf{s})l_z - 2l_z s_z - \mathbf{l} \cdot \mathbf{s}$.

4.4. Quadrupole sum rule for in-plane XMLD (xyXMLD)

Next, we consider $l = 2$ and $m = \pm 2$ cases, $S_{2,\pm 2}^{j\pm} = \frac{3}{\sqrt{15}} P_{\pm 1, \mp 1}^{j\pm}$, corresponding to the cross term of left and right circular polarization, which is not possible to directly observe in absorption which can only describe the polarization of the incident x-rays as shown in Equation (9). Therefore, we consider the combination of sum rules for $m = \pm 2$, and then it becomes clear that the signal can be observed as an in-plane xyXMLD [$I_{xy\text{XMLD}}^{j\pm} = I_x^{j\pm} - I_y^{j\pm}$] component using $S_{2,2}^{j\pm} + S_{2,-2}^{j\pm} = \frac{3}{\sqrt{15}} (I_x^{j\pm} - I_y^{j\pm})$. The corresponding spinless multipole of quadrupole moment is given by $\underline{Q}_{2,2}^{(\text{orb})} + \underline{Q}_{2,-2}^{(\text{orb})}$; consequently, the spinless sum rule is expressed as

$$I_{xy\text{XMLD}}^{j+} + I_{xy\text{XMLD}}^{j-} = \langle \underline{Q}_{x^2-y^2} \rangle C, \quad (34)$$

with the operator equivalent $\underline{Q}_{x^2-y^2} \equiv (l_y^2 - l_x^2)/6$, reflecting the anisotropic charge distribution within the xy -plane.

The spinful electronic quadrupole moments are composed of magnetic dipole and octupole terms. The magnetic dipole one is given by

$$Q_{x^2-y^2}^{(1,-1)} \equiv Q_{2,2}^{(1,-1)} + Q_{2,-2}^{(1,-1)} = \frac{1}{2} (l_x s_x - l_y s_y) \quad (35)$$

with $Q_{2,\pm 2}^{(1,-1)} = \sum_n C_{1,\pm 2-n;1n}^{2,\pm 2} M_{1,\pm 2-n}^{(\text{orb})} \sigma_{1n}$, indicating the anisotropy of the spin-orbit coupling within the xy -plane. On the other hand, the octupole term is expressed as

$$Q_{2,\pm 2}^{(1,1)} = - \sum_n C_{3,\pm 2-n;1n}^{2,\pm 2} M_{3,\pm 2-n}^{(\text{orb})} \sigma_{1n} \quad (36)$$

where the magnetic octupole operators are given in Table 2. For example, when the

spin is oriented along the z -axis, extracting only the term proportional to s_z results in

$$(M_{3,2}^{(\text{orb})} + M_{3,-2}^{(\text{orb})})\sigma_z = \sqrt{\frac{15}{2}}[xzl_x - yzl_y]_+s_z + (x^2 - y^2)l_zs_z, \quad (37)$$

which reflects a quantity combining the electric quadrupole and spin-orbit coupling involving the in-plane anisotropy. Consequently, the spinful sum rule for xyXMLD is expressed as

$$I_{\text{xyXMLD}}^{j+} - 2I_{\text{xyXMLD}}^{j-} = \left(\frac{2}{5}\langle P_{x^2-y^2} \rangle + \frac{3}{5}\langle R_{x^2-y^2} \rangle \right) C, \quad (38)$$

with the operator equivalents $P_{x^2-y^2} \equiv \frac{2}{3}(l_x s_x - l_y s_y)$ and $R_{x^2-y^2} \equiv \frac{2}{9}\{l_y(\mathbf{l} \cdot \mathbf{s})l_y - l_x(\mathbf{l} \cdot \mathbf{s})l_x\}$. Since these electric quadrupole moments have same symmetry as the magnetic toroidal quadrupole moment with applied magnetic field, it is expected to detect the anisotropy of the electronic states in d -wave altermagnets [42, 43].

5. Conclusion

In this study, we have reconsidered the sum rules for X-ray absorption spectroscopy based on a complete magnetic multipole basis. We have demonstrated that it naturally derives the anisotropic magnetic dipole term in the XMCD, which plays important role in the s -wave altermagnetic system. Additionally, we have shown that the sum rules for out-of-plane and in-plane X-ray Magnetic Linear Dichroism (XMLD) can be derived using the electric quadrupole contributions. This approach provides a unified theoretical framework to analyze and interpret dichroic signals in a wide range of magnetic materials. Our findings not only enhance the understanding of XMCD and XMLD but also pave the way for further research in complex magnetic structures. Future studies incorporating this multipole-based methodology could further refine our insights into spin-orbit interactions and hidden magnetic orderings in advanced magnetic materials.

6. Acknowledgment

The authors thank T. Arima and M. Mizumaki for the productive discussion. This project is partly supported by the Japan Society for the Promotion of Science (JSPS) KAKENHI (19H04399, 24K03205, and 24H01685). This work was supported by MEXT Quantum Leap Flagship Program (MEXT Q-LEAP) Grant Number JPMXS0118068681. This work is also partially supported by CREST(JPMJCR1861 and JPMJCR2435), Japan Science and Technology Agency (JST).

References

- [1] F. M. F. de Groot and A. Kotani, *Core Level Spectroscopy of Solids* (Cambridge University Press, 2008) ISBN: 978-0521831793.
- [2] G. Schütz, W. Wagner, W. Wilhelm, P. Kienle, R. Zeller, R. Frahm, and G. Materlik, Phys. Rev. Lett. **58**, 737 (1987).

- [3] J. Stöhr, *J. Magn. Magn. Mater.* **200**, 470 (1999).
- [4] D. Alders, L. H. Tjeng, F. C. Voogt, T. Hibma, G. A. Sawatzky, C. T. Chen, J. Vogel, M. Sacchi, and S. Iacobucci, *Phys. Rev. B* **57**, 11623 (1998).
- [5] G. van der Laan and A. I. Figueira, *Coord. Chem. Rev.* **277–278**, 95 (2014).
- [6] B. T. Thole, P. Carra, F. Sette, and G. van der Laan, *Phys. Rev. Lett.* **68**, 1943 (1992).
- [7] P. Carra, B. T. Thole, M. Altarelli, and X. Wang, *Phys. Rev. Lett.* **70**, 694 (1993).
- [8] C. T. Chen, Y. U. Idzerda, H.-J. Lin, N. V. Smith, G. Meigs, E. Chaban, G. H. Ho, E. Pellegrin, and F. Sette, *Phys. Rev. Lett.* **75**, 152 (1995).
- [9] Y. Teramura, A. Tanaka, and T. Jo, *Journal of the Physical Society of Japan* **65**, 1053 (1996).
- [10] C. Bi, Y. Liu, T. Newhouse-Illige, M. Xu, M. Rosales, J. W. Freeland, O. Mryasov, S. Zhang, S. G. E. te Velthuis, and W. G. Wang, *Phys. Rev. Lett.* **113**, 267202 (2014).
- [11] B. Zhang, C.-J. Sun, W. Lü, T. Venkatesan, M.-G. Han, Y. Zhu, J. Chen, and G. M. Chow, *Phys. Rev. B* **91**, 174431 (2015).
- [12] S. Miwa, K. Matsuda, K. Tanaka, Y. Kotani, M. Goto, T. Nakamura, and Y. Suzuki, *Applied Physics Letters* **107**, 162402 (2015).
- [13] S.-J. Chang, M.-H. Chung, M.-Y. Kao, S.-F. Lee, Y.-H. Yu, C.-C. Kaun, T. Nakamura, N. Sasabe, S.-J. Chu, and Y.-C. Tseng, *ACS Applied Materials & Interfaces* **11**, 31562 (2019).
- [14] Y. Ishii, Y. Yamasaki, Y. Kozuka, J. Lustikova, Y. Nii, Y. Onose, Y. Yokoyama, M. Mizumaki, J.-i. Adachi, H. Nakao, T.-h. Arima, and Y. Wakabayashi, *Scientific reports* **14**, 15504 (2024).
- [15] C. T. Chen, F. Sette, Y. Ma, and S. Modesti, *Phys. Rev. B* **56**, R4959 (1997).
- [16] A. Scholl, J. Stohr, J. Luning, J. W. Seo, J. Fompeyrine, H. Siegwart, J.-P. Locquet, F. Nolting, S. Anders, E. Fullerton, *et al.*, *Science* **287**, 1014 (2000).
- [17] L. Šmejkal, R. Gonzalez-Hernandez, T. Jungwirth, and J. Sinova, *Sci. Adv.* **6**, eaba9399 (2020).
- [18] L. Šmejkal, R. Gonzalez-Hernandez, T. Jungwirth, and J. Sinova, *Science* **375**, 70 (2022).
- [19] L. Šmejkal, T. Jungwirth, and J. Sinova, *Nat. Rev. Mater.* **8**, 653 (2023).
- [20] I. V. Solovyev, *Phys. Rev. B* **55**, 8060 (1997).
- [21] Y. Noda, K. Ohno, and S. Nakamura, *Phys. Chem. Chem. Phys.* **18**, 13294 (2016).
- [22] T. Okugawa, K. Ohno, Y. Noda, and S. Nakamura, *Journal of Physics: Condensed Matter* **30**, 075502 (2018).
- [23] K.-H. Ahn, A. Hariki, K.-W. Lee, and J. Kuneš, *Phys. Rev. B* **99**, 184432 (2019).
- [24] M. Naka, S. Hayami, H. Kusunose, Y. Yanagi, Y. Motome, and H. Seo, *Nature Communications* **10** (2019).
- [25] Y. Yamasaki, H. Nakao, and T.-h. Arima, *Journal of the Physical Society of Japan* **89**, 083703 (2020).
- [26] N. Sasabe, M. Kimata, and T. Nakamura, *Phys. Rev. Lett.* **126**, 157402 (2021).
- [27] M. Kimata, N. Sasabe, K. Kurita, Y. Yamasaki, C. Tabata, Y. Yokoyama, Y. Kotani, M. Ikhlas, T. Tomita, K. Amemiya, H. Nojiri, S. Nakatsuji, T. Koretsune, H. Nakao, T.-h. Arima, and T. Nakamura, *Nat. Commu.* **12**, 5582 (2021).
- [28] S. Sakamoto, T. Higo, M. Shiga, K. Amemiya, S. Nakatsuji, and S. Miwa, *Physical Review B* **104**, 134431 (2021).
- [29] S. Sakamoto, T. Higo, Y. Kotani, H. Kosaki, T. Nakamura, S. Nakatsuji, and S. Miwa, *Physical Review B* **110**, L060412 (2024).
- [30] A. Hariki, A. Dal Din, O. J. Amin, T. Yamaguchi, A. Badura, D. Kriegner, K. W. Edmonds, R. P. Campion, P. Wadley, D. Backes, L. S. I. Veiga, S. S. Dhesi, G. Springholz, L. Šmejkal, K. Výborný, T. Jungwirth, and J. Kuneš, *Phys. Rev. Lett.* **132**, 176701 (2024).
- [31] O. J. Amin, A. D. Din, E. Golias, Y. Niu, A. Zakharov, S. C. Fromage, C. J. B. Fields, S. L. Heywood, R. B. Cousins, F. Maccherozzi, J. Krempaský, J. H. Dil, D. Kriegner, B. Kiraly, R. P. Campion, A. W. Rushforth, K. W. Edmonds, S. S. Dhesi, L. Šmejkal, T. Jungwirth, and P. Wadley, *Nature* **636**, 348 (2024).

[32] H. Kusunose, R. Oiwa, and S. Hayami, Journal of the Physical Society of Japan **89**, 104704 (2020).

[33] S. Hayami and H. Kusunose, Journal of the Physical Society of Japan **93**, 072001 (2024).

[34] Here, we use the following relation, $\sum_{m_j} C_{l_c m_c; \frac{1}{2} m_s}^{j m_j} C_{l_c m'_c; \frac{1}{2} m'_s}^{j m_j} = \frac{j \pm \frac{1}{2}}{2l_c + 1} C_{\frac{1}{2} m'_s; 00}^{\frac{1}{2} m_s} C_{l_c m'_c; 00}^{l_c m_c} \pm \sum_{n=-1}^1 \frac{\sqrt{3l_c(l_c+1)}}{2l_c + 1} C_{\frac{1}{2} m'_s; 1n}^{\frac{1}{2} m_s} C_{l_c m'_c; 1, -n}^{l_c m_c}.$

[35] The function for finite summation involving four Clebsh-Gordan coefficients used here is found in <https://functions.wolfram.com/07.38.23.0029.01>.

[36] P. Carra, H. König, B. Thole, and M. Altarelli, Physica B: Condensed Matter **192**, 182 (1993).

[37] T. Oguchi and T. Shishidou, Phys. Rev. B **70**, 024412 (2004).

[38] G. van der Laan, Phys. Rev. B **57**, 112 (1998).

[39] N. Sasabe, M. Mizumaki, T. Uozumi, and Y. Yamasaki, Physical Review Letters **131**, 216501 (2023).

[40] S. Hayami and H. Kusunose, Phys. Rev. B **103**, L180407 (2021).

[41] G. van der Laan, Physical review letters **82**, 640 (1999).

[42] T. Higuchi and M. Kuwata-Gonokami, Nature communications **7**, 10720 (2016).

[43] H. Koizumi, Y. Yamasaki, and H. Yanagihara, Nature Communications **14**, 8074 (2023).